Electronic Supplementary Material (ESI) for Journal of Materials Chemistry C.
This journal is © The Royal Society of Chemistry 2021

Supporting Information

Single-molecule Conductance Variations up to Four Orders of Magnitudes via Contacting Electrodes with Different Anchoring Sites

Zhiyu Zhu,[a] Hang Qu,[a] Yaorong Chen,[a] Chengyang Zhang, [a] Ruihao Li,[a] Yi Zhao,[a] Yu Zhou,[a] Zhixin Chen,*[a, b] Junyang Liu,[a] Zongyuan Xiao,*[a] and Wenjing Hong*[a]

[a] State Key Laboratory of Physical Chemistry of Solid Surfaces, iChEM, College of Chemistry and Chemical Engineering, Xiamen University, Xiamen 361005, China
[b] Department of Materials, University of Oxford, Parks Road, Oxford OX1 3PH, United Kingdom
E-mail: zhixin.chen@materials.ox.ac.uk ; xiaozy@xmu.edu.cn; whong@xmu.edu.cn

State Key Laboratory of Physical Chemistry of Solid Surfaces, College of Chemistry and Chemical Engineering, Collaborative Innovation

Center of Chemistry for Energy Materials, Xiamen University, Xiamen, Fujian 361005, China
State Key Laboratory of Physical Chemistry of Solid Surfaces, College of Chemistry and Chemical Engineering,
Collaborative Innovation Center of Chemistry for Energy Materials, Xiamen University, Xiamen, Fujian 361005, China

Table of Contents

1. Single-molecule Junction Measurement 2
2. Theoretical Calculations 5
3. Synthesis Information 7
Reference 12

1. Single-molecule Junction Measurement

In this work, we constructed the molecular junction by a home-built scanning tunneling microscope break junction (STM-BJ). The gold tips were fabricated using the gold wires (99.99 %, 0.25 mm diameter), which were purchased from Beijing Jiaming Platinum Nonferrous Metal Co. Ltd. The gold wires were burned to be bead when used and it was attached to the piezo. The gold was evaporated on a silicon wafer to fabricate the substrate, which was placed below the tips. The substrate was pre-washed by piranha solution (v(H_2SO_4): v(H_2O_2) = 3:1) for about four hours and washed by fresh deionized water three times. Before the experiment, calibration was conducted in pure solvent to acquire accurate conductance information versus distance which is showed in Fig. S1. According to the Landauer equation:

$$G = G_0 e^{-\beta_T z}$$

Where β_T represents the transmission coefficient in the pure solvent environment, z is the distance between the two gold electrodes. Account of the fact that we record the relative distance in the experiment, then the equation can be transformed to

$$\log\left(\frac{\Delta G}{G_0}\right) = -0.434\beta_T(z - z_{corr})$$

Where z_{corr} is the length of the snap-back effect, therefore, the transmission coefficient and the exact length of the snap-back effect in the solvent environment could be inferred by measuring the conductance change in the pure solvent environment. Then, 50 μL 1,2,4-trichlorobenezen (TCB) solution containing 0.1 mmol target molecule was dripped on the substrate, and the tip was also immersed in the solution. The current and

voltage data were collected to analyze the conductance. The plateau length histograms of every possible conductance for both **TPE-m-OH** and **TPE-p** are presented in Fig. S2. The construction method of 1D/2D conductance and PSD analysis histogram can refer to some previous work.[1–3]

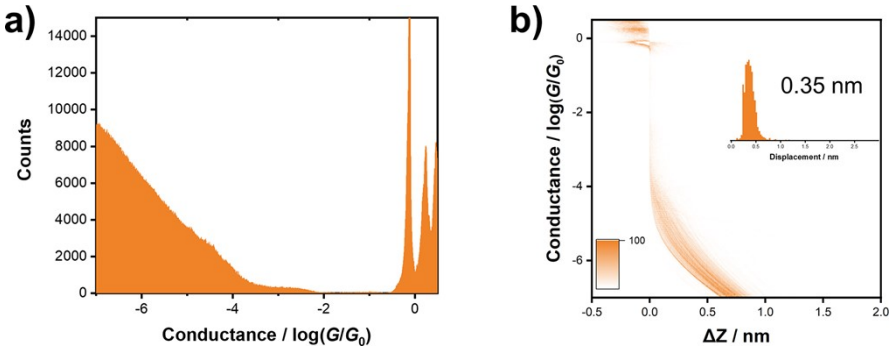

Fig. S1 (a) 1D conductance histogram and (b) 2D conductance versus relative displacement histogram of the pure TCB.

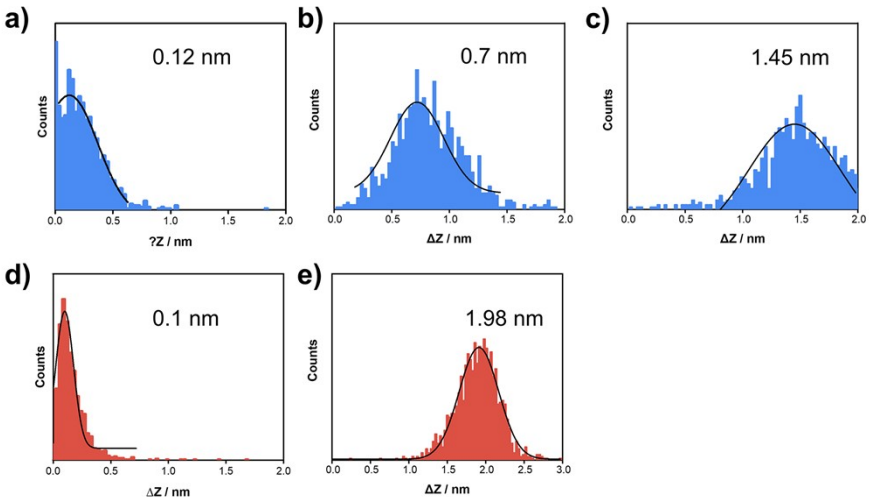

Fig. S2 (a-c) The plateau length histogram of **TPE-m-OH** for high (a), medium (b) and low (c) conductance. (d-e) The plateau length histogram of **TPE-p** for high (d) and low (e) conductance.

Flicker noise of molecule conductance traces were measured to distinguish different mechanisms of charge transport through the molecular junctions. According to the previous studies,[4] the noise power spectrum density (PSD) is proportional to the G^n. If the number of n is closer to 1, then the molecule is through-bond mechanism dominated. In the experiment, we calculated the average conductance G_{avg} and PSD of every trace during the suspending time, and the exponent n can be obtained when the correlation of the PSD and PSD/ G^n is 0, which can be calculated according to the formula below.

$$n = argmin_n \left| corrcoef\left(G_{avg}, \frac{PSD}{G_{avg}^{\ n}}\right)\right|$$

The typical individual hover conductance traces and normalized conductance change versus normalized noise power were presented in Fig S3.

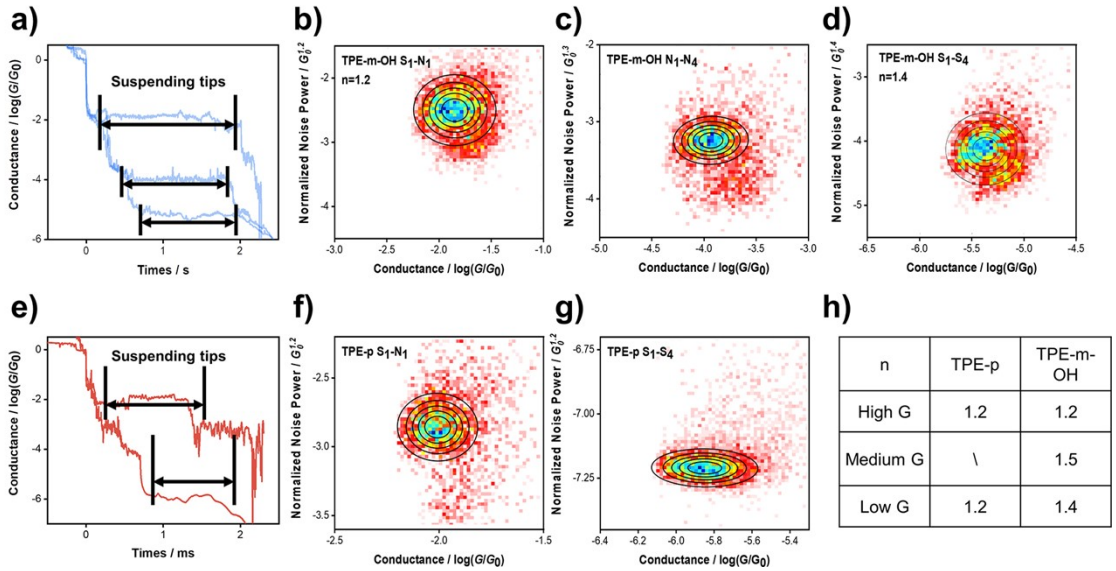

n	TPE-p	TPE-m-OH
High G	1.2	1.2
Medium G	\	1.5
Low G	1.2	1.4

Fig. S3 (a, e) Typical individual hover conductance traces of **TPE-m-OH** (blue) and **TPE-p** (red). (b-d, f-g) Two-dimensional histogram of normalized conductance change versus normalized noise power for **TPE-m-OH** (b-d), **TPE-p** (f-g). (h) Statistics for values of normalized parameter n under different conductance.

Correlation analysis was used to reveal the relationship between multiple conductance signals. We constructed the correlation histogram of a sliding square window, and the trace was divided into a sliding square window with a length of 0.1 nm. The correlation coefficients value p was calculated through the Pearson correlation between the previous window and the subsequent window. The results of both 1,2,4-trichlorobenezen (TCB) solution containing 0.1 mM of molecules (a,c) and with the mixture of 0.1 mM of molecules with 0.1 mM of 4-(Methylthio)aniline were presented in Fig. S4.

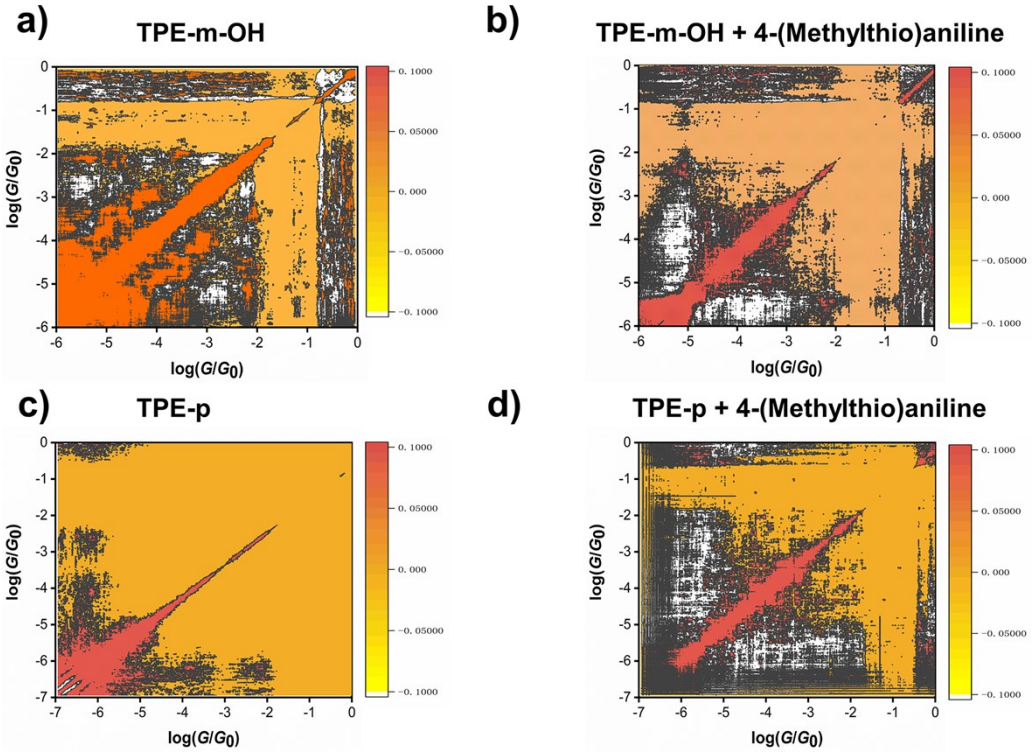

Fig. S4 Correlation histogram of conductance for **TPE-m-OH**, **TPE-p** and their mixed solution with 4-(Methylthio)aniline.

2. Theoretical Calculations

In order to simplify the model, a para-substituted benzene model was constructed as Fig. S5. All structures are optimized using Gaussian with the B3LYP hybrid functional and the 6-31g* basis sets. The energy-dependent transmission coefficient *T*(E) is calculated using density functional theory (DFT) combined with non-equilibrium green's function (NEGF) formalism by Atomic Tool Kit (ATK) software package.[5–7] The optimized molecules are used to construct the model of a single-molecule device. The initial distance of Au-S and Au-N is set to be 2.65 Å and 2.45 Å as in previous works. Those models are optimized by Siesta to broaden the scattering region until all atoms are more petite than 0.05eV/Å. Then, the transmission coefficient is calculated by ATK, and the transmission spectra dependent on the energy of molecular orbitals can also be obtained. The binding energy was calculated by the single point task at ωB97XD level after the geometry optimization by Gaussian, 6-31g* basis set was used for **TPE-m-OH** and **TPE-p** and SDD was used for gold.

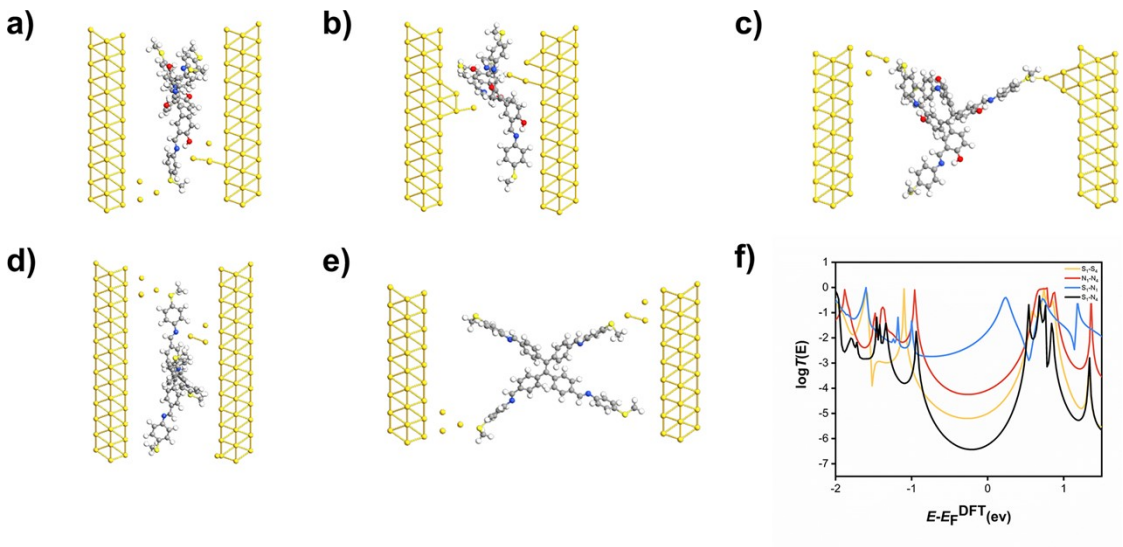

Fig. S5 (a-e) The optimized molecular device structures of **TPE-p** and **TPE-m-OH**. (f) The transmission spectrum of S_1-N_4 anchoring sites for **TPE-m-OH**.

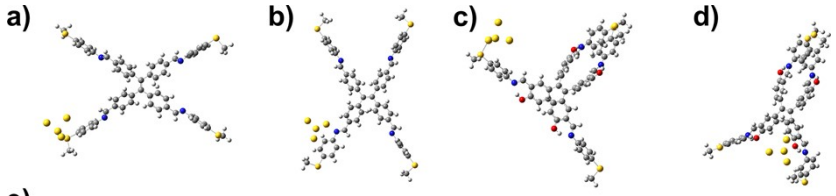

e)

Binding Energy	TPE-p	TPE-m-OH
Au-S	-39.26 kcal/mole	-42.09 kal/mole
Au-N	-46.96 kcal/mole	-51.08 kcal/mole

Fig. S6 The binding energy of different anchoring structures of **TPE-p** and **TPE-m-OH**.

Table. S1. Theoretical molecule length

	TPE-m-OH	TPE-p
High G	0.6 nm	0.6 nm
Medium G	1.2 nm	\
Low G	1.9 nm	2.5 nm

3. Synthesis Information

Synthesis steps of TPE-p.

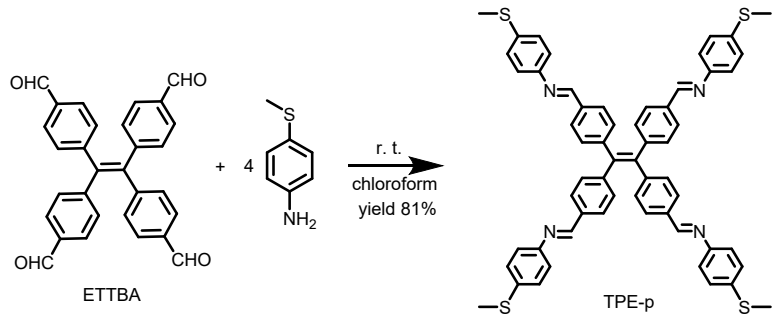

TPE-p was synthesized from 4,4′,4″,4‴-(ethene-1,1,2,2-tetrayl)-tetrabenzaldehyde (ETTBA) through imine condensation. ETTBA has been reported in the previous literature.[8] ETTBA (44.4 mg, 0.1 mmol, 1 equiv.) was mixed with 4-(methylthio)aniline (55.6 mg, 0.4 mmol, 4 equiv.) in chloroform at ambient temperature. After 24 h, the crude solution was evaporated in vacuum and recrystallized in ethanol/ chloroform to afford yellow powder (yield 81%).

^{1}H NMR (600 MHz, $CDCl_3$) δ 8.40 (s, 4H), 7.69 (d, J = 8.3 Hz, 8H), 7.29-7.26 (m, 8H), 7.20-7.16 (m, 8H), 7.17-7.14 (m, 8H), 2.50 (d, J = 4.2 Hz, 12H).

Synthesis steps of TPE-m-OH.

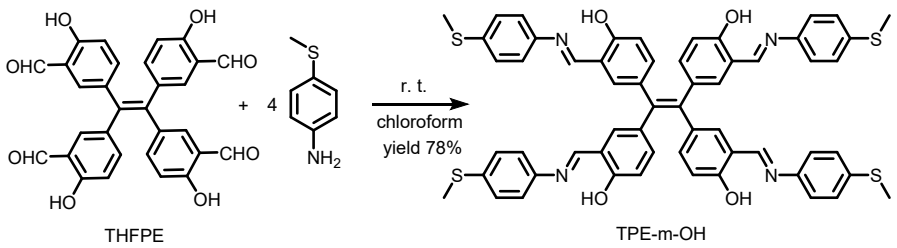

TPE-m-OH was synthesized from the meta-aldehyde TPE (THFPE) through imine condensation. THFPE has also been reported in the previous literature. [9] THFPE (50.8 mg, 0.1 mmol, 1 equiv.) and 4-(methylthio)aniline (55.6 mg, 0.4 mmol, 4 equiv.) was mixed in chloroform at room temperature overnight. The crude solution was evaporated in vacuum and recrystallized in ethanol/chloroform to afford dark red powder (yield 78%).

^{1}H NMR (600 MHz, $CDCl_3$) δ 13.33 (s, 4H), 8.43 (s, 4H), 7.30- 7.29 (d, *J* = 2.4 Hz, 4H), 7.28 (d, *J* = 2.4 Hz, 4H), 7.22-7.20 (m, 8H), 7.14 (dd, *J* = 8.4, 2.2 Hz, 5H), 7.12 (d, *J* = 2.1 Hz, 4H), 6.83 (d, *J* = 8.4 Hz, 4H), 2.52 (s, 12H).

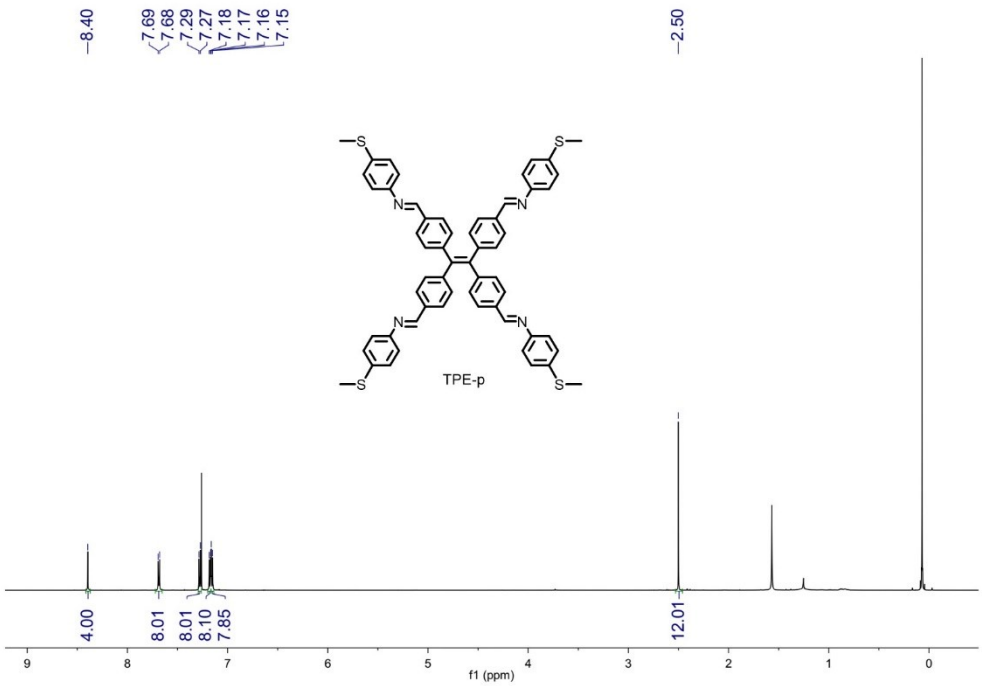

Fig. S5. ^{1}H-NMR of **TPE-p** (600 MHz, $CDCl_3$).

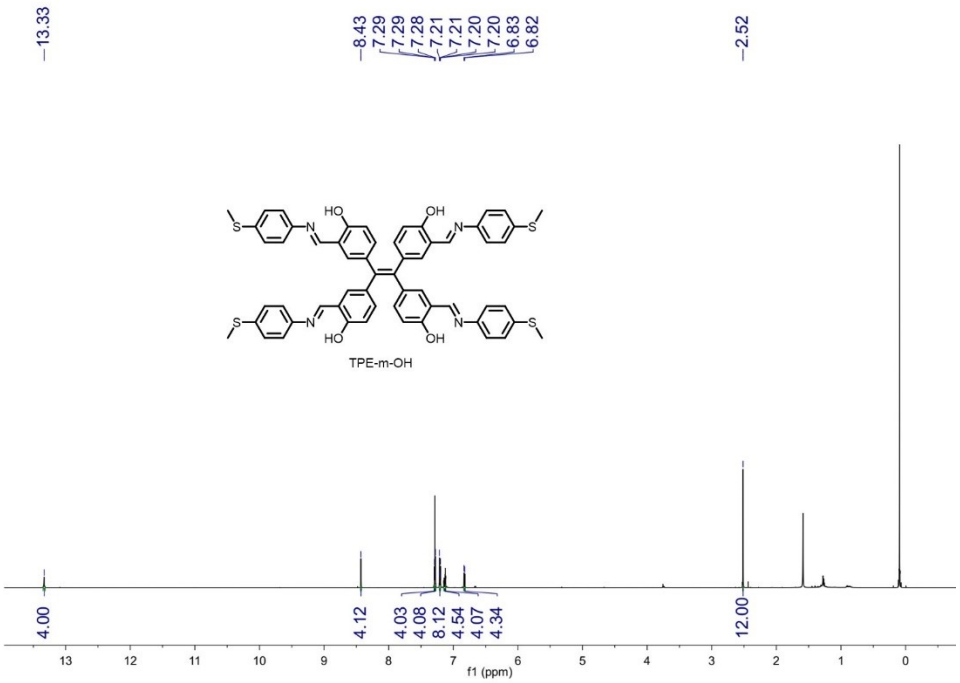

Fig S6. ^{1}H-NMR of **TPE-m-OH** (600 MHz, $CDCl_3$).

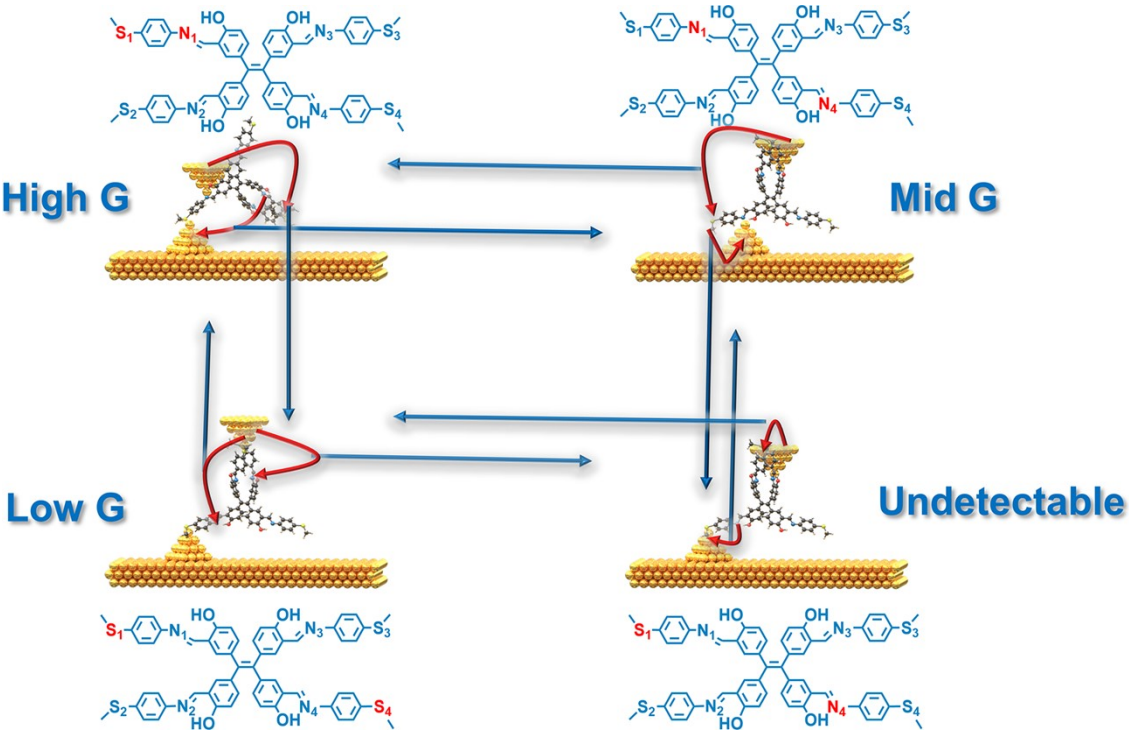

Fig. S7 The schematic diagram of the mechanism of the transitions between different conductance states for the single molecule mechanical switch.

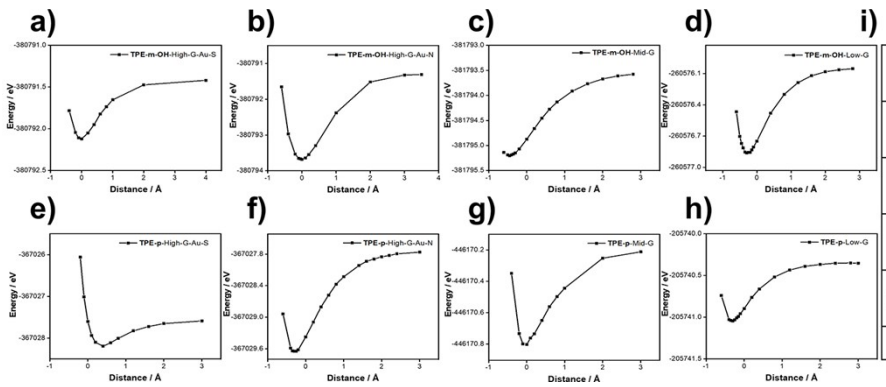

i)

Adsorption Energy		
	TPE-m-OH	TPE-p
High G – Au-S	-0.70 eV	-0.60 eV
High G – Au-N	-2.50 eV	-1.85 eV
Medium G	-1.63 eV	-0.59 eV
Low G	-0.81 eV	-0.70 eV

Fig. S8 (a-d) The diagram of energy versus distance between the molecule and gold electrode for **TPE-m-OH** of all possible anchoring sites. (e-h) The diagram of energy versus distance between the molecule and gold electrode for **TPE-p** of all possible anchoring sites. (i) The adsorption energy for **TPE-m-OH** and **TPE-p**.

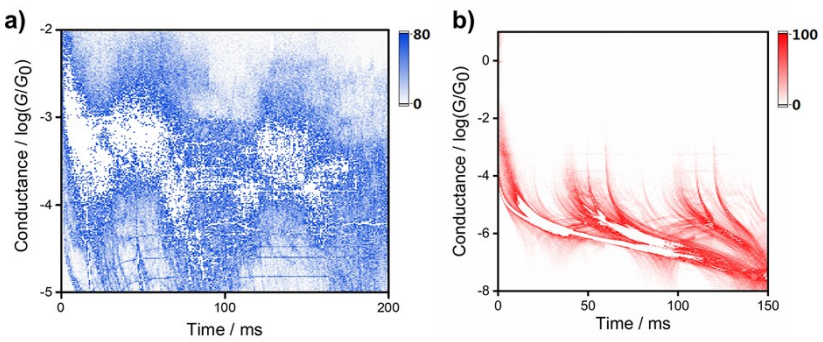

Fig. S9 (a) A 2D histogram constructed from selected traces for OPE-3 of compression–elongation experiments. (b) A 2D histogram constructed from selected traces for pure solvent of compression–elongation experiments.

The SHINERS technique has been performed to characterize these two molecules. We assigned the low-frequency bands at 411 cm^{-1} and 410 cm^{-1} to the N−Au stretching vibrations for TPE-m-OH and TPE-p.[10] However, the S-Au stretching vibrations in 200~300 [11] is hardly to be observed, which may result from the reason that the molecule lies flat on the electrode, which is similar with previous research.[12,13]

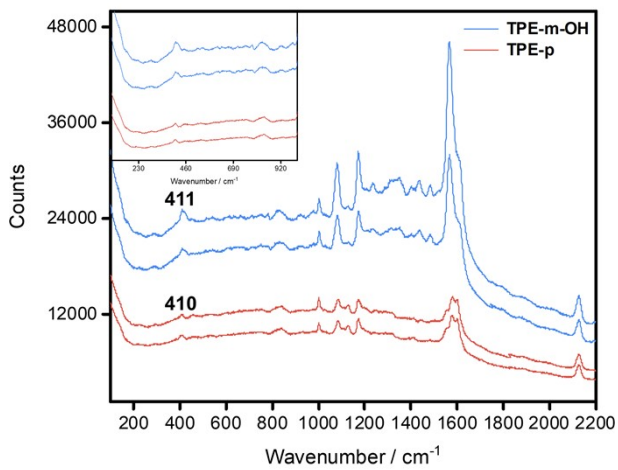

Fig. S10 The SHINERS results of **TPE-m-OH** and **TPE-p**.

Reference

1 O. Adak, E. Rosenthal, J. Meisner, E. F. Andrade, A. N. Pasupathy, C. Nuckolls, M. S. Hybertsen and L. Venkataraman, *Nano Lett.*, 2015, **15**, 4143–4149.

2 Y. Song and T. Lee, *J. Mater. Chem. C*, 2017, **5**, 7123–7141.

3 Z. Chen, L. Chen, G. Li, Y. Chen, C. Tang, L. Zhang, J. Liu, L. Chen, Y. Yang, J. Shi, J. Liu, H. Xia and W. Hong, *Cell Reports Physical Science*, 2021, **2**, 100329.

4 C. Tang, L. Chen, L. Zhang, Z. Chen, G. Li, Z. Yan, L. Lin, J. Liu, L. Huang, Y. Ye, Y. Hua, J. Shi, H. Xia and W. Hong, *Angew. Chem. Int. Ed.*, 2019, **58**, 10601–10605.

5 K. S. Thygesen and K. W. Jacobsen, *Chem. Phys.*, 2005, **319**, 111–125.

6 Z. Li, M. Smeu, S. Afsari, Y. Xing, M. A. Ratner and E. Borguet, *Angew. Chem. Int. Ed.*, 2014, **53**, 1098–1102.

7 G. C. Solomon, C. Herrmann, T. Hansen, V. Mujica and M. A. Ratner, *Nat. Chem.*, 2010, **2**, 223–228.

8 H. Qu, Y. Wang, Z. Li, X. Wang, H. Fang, Z. Tian and X. Cao, *J. Am. Chem. Soc.*, 2017, **139**, 18142–18145.

9 H. Qu, X. Tang, X. Wang, Z. Li, Z. Huang, H. Zhang, Z. Tian and X. Cao, *Chem. Sci.*, 2018, **9**, 8814–8818.

10 R. Holze, *J. Electroanal. Chem.*, 1988, **250**, 143–157.

11 K. T. Carron and L. G. Hurley, *J. Phys. Chem.*, 1991, **95**, 9979–9984.

12 B. Heinz and H. Morgner, *Surface Science*, 1997, **372**, 100–116.

13 D. P. Fromm, A. Kinkhabwala, P. J. Schuck, W. E. Moerner, A. Sundaramurthy and G. S. Kino, *J. Chem. Phys.*, 2006, **124**, 61101.